# Identification of Feasible Scaled Teleoperation Region Based on Scaling Factors and Sampling Rates

**Dal-Yeon Hwang\***
*Department of Mechanical Design Engineering, Korea Polytechnic University*
**Blake Hannaford**
*Department of Electrical Engineering, Biorobotics Laboratory, University of Washington*
**Hyoukryeol Choi**
*Department of Mechanical Engineering, SungKyunKwan University*

The recent spread of scaled telemanipulation into microsurgery and the nano-world increasingly requires the identification of the possible operation region as a main system specification. A teleoperation system is a complex cascaded system since the human operator, master, slave, and communication are involved bilaterally. Hence, a small time delay inside a master and slave system can be critical to the overall system stability even without communication time delay. In this paper we derive an upper bound of the scaling product of position and force by using Llewellyn's unconditional stability. This bound can be used for checking the validity of the designed bilateral controller. Time delay from the sample and hold of computer control and its effects on stability of scaled teleoperation are modeled and simulated based on the transfer function of the teleoperation system. The feasible operation region in terms of position and force scaling decreases sharply as the sampling rate decreases and time delays inside the master and slave increase.

**Key Words** : Scaled Teleoperation or Telemanipulation, Position and Force Scaling, Upper Bound of Scaling, Digital Control Model, Llewellyn's Unconditional Stability

**Nomenclature** ─────────────

| | |
|---|---|
| M | : Master |
| S | : Slave |
| MS | : Master and slave |
| H.O. | : Human operator |
| $S_p$ | : Position scaling gain from M to S |
| $S_f$ | : Force scaling gain from S to M |
| r | : Adjusting force scaling constant |
| $G_{mp}$ | : Master plant model |
| $G_{rp}$ | : Slave plant model |
| $x_m/v_m$ | : Master position/master velocity |
| $x_r/v_r$ | : Slave position/slave velocity |

| | |
|---|---|
| $b_m$ | : Friction compensation coefficient for M |
| $b_r$ | : Friction compensation coefficient for S |
| $T_s$ | : Sampling time |
| $f_s$ | : Sampling frequency |
| $D(z)$ | : Discrete differentiator for velocity induction |
| Fh | : Human operator force |
| Fe | : Environment force |
| $g_f$ | : force reflection gain from S to M |
| LPF | : low pass filter |
| $g_p$ | : Coordinate torque gain to M |

Subscript 'r' is used for slave side instead of 's' to avoid confusion with Laplace operator, s.

\* Corresponding Author,
　**E-mail** : dyhwang@kpu.ac.kr
　**TEL** : +82-31-496-8228 ; **FAX** : +82-31-496-8239
　Department of Mechanical Design Eng., Korea Polytechnic University, 3Ga-101, Jungwang-dong, Shihung-city, Kyunggi-do 429-793, Korea. (Manuscript **Received** June 17, 1999; **Revised** October 17, 2000)

## 1. Introduction

Scaled teleoperation or telemanipulation is a subset of teleoperation, with the capability of scaling in factors such as force, position,

impedance and power (Hannaford, 1989). Recent applications to the micro or nano-world like microsurgery, which belongs to the macro-micro bilateral manipulation category(MMBM) (Kobayashi and Nakamura, 1992, Fukuda et al., 1987, Colgate, 1991), shows the effectiveness of scaled teleoperation.

A teleoperation system is composed of several parts such as a human operator, master robot or handle (M), communication channel, slave or remote robot (S) and object to be handled. The multiple part makes the identification of the feasible operation region of scaled teleoperation very difficult due to accumulation of model errors and time delays in and out of M and S. The operative region is limited by stability and performance (Raju et. al., 1989, Hannaford, 1989, Lawn et al., 1993, Hwang et. al., 1994). Stability problem due to pure communication time delay between the master and slave which is critical to space operation, was solved using a lossless transmission line analogy (Anderson and Spong, 1988). Thereafter, this passivity approach has been popular among researchers. However, this passivity-based control can lower performance up to 50% according to (Lawn and Hannaford, 1993). One of the reasons is due to low force reflection gain for the master. It is shown that position error-based force reflection combined with compliance control resulted in the best task performance when the set of a normal master and a large and stiff slave robot was used (Kim, 1992). The overall system stability depends on both the communication channel time delay and the sampling rate of each of the single systems, M and S. To know the feasible operation region in terms of scaling factors, such as position or force, can be more helpful to a human operator (H.O.) as MMBM spreads. So far, there have been few papers showing how the feasible operation region depends on position and force scaling factors and sampling rates in nonidentical master and slave robots.

In this paper, we derive an upper bound for the scaling gain product of position and force based on the unconditional stability in the frequency domain. We then identify the stable or feasible region of scaled teleoperation in terms of force,

position scaling and sampling rates based on the characteristic equation when the time delay in each M and S are assumed to be from 0 to three sampling times (Ts). To include the time delay from sampling rates we used a digital control model.

## 2. Upper Bound of Scaling

### 2.1 Two-Port network H matrix building

In this section we derive the upper bound of the product of position and force scaling based on a two-port network passivity approach and Llewellyn's stability criteria (Adams et. al., 1999). The two-port network shape of a scaled teleoperation system is shown in Fig. 1. This has the feature of simplicity with no impedance shaping (Colgate, 1994). We added a force feedback line from the coordinated control input of the slave, $g_p$ (Fig. 1). We can refer to more general control models from (Strassberg, 1992). In scaled teleoperation, the master and slave are usually different in kinematic structure and dynamics, and the control method depending on the intended use.

For the identification of scaling, we chose the unconditional stability criteria for the following reasons :

1) At the terminating points of M and H.O. or S and the environment, we can assume one-port instead of two-port terminations.

2) Llewellyn (LL)'s criteria, which is less conservative for stability than the passivity condition (Adams and Hannaford, 1999) can provide a decoupled form for the scaling product.

$$\text{Re}(p_{11}) \geq 0 \tag{1}$$
$$\text{Re}(p_{22}) \geq 0 \tag{2}$$
$$2\text{Re}(p_{11})\text{Re}(p_{22}) \geq |p_{12}p_{21}| + \text{Re}(p_{12}p_{21}) \tag{3}$$
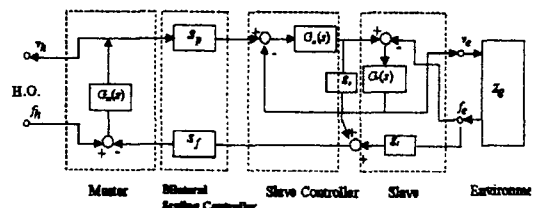


**Fig. 1**    Bilateral control of a scaled teleoperation in two-port network shape

$\forall \omega \geq 0$

Define the matrix

$$P = \begin{bmatrix} p_{11} & p_{12} \\ p_{21} & p_{22} \end{bmatrix}$$

to be the immittance matrix of the two-port network system. P can be a matrix such as the impedance Z, admittance Y, or hybrid H. We chose the H matrix as the immitance and derive the H parameters of Fig. 1 as follows before identifying the upperbound of scaling.

$$h_{11} = \frac{1}{G_m} + s_p s_f (g_p G_c)\left(1 - \frac{G_c G_r}{G_c G_r + 1}\right)$$

$$h_{12} = s_f\left(g_f + g_p \frac{G_c G_r}{G_c G_r + 1}\right)$$

$$h_{21} = -s_p\left(\frac{G_c G_r}{G_c G_r + 1}\right)$$

$$h_{22} = \frac{G_r}{1 + G_c G_r}$$

These h-parameters can have another form according to the control architecture. However, we can observe that the scaling gains of $s_p$ and $s_f$ in $h_{12}$, $h_{21}$ are in the product form with additional functions while these gains with extra functions are added to the master impedance.

$$P = \begin{bmatrix} \frac{1}{G_m} + s_p s_f g_p G_c\left(1 - \frac{G_c G_r}{1 + G_c G_r}\right) & s_f\left(g_f + g_p \frac{G_c G_r}{1 + G_c G_r}\right) \\ -s_p\left[\frac{G_c G_r}{1 + G_c G_r}\right] & \frac{G_r}{1 + G_c G_r} \end{bmatrix}$$

$$= \begin{bmatrix} z_m + r_0 E & s_f F \\ -s_p D & J \end{bmatrix} \quad (4)$$

## 2.2 Upper bound of scaling by unconditional stability

If we apply Llewellyn (LL)'s unconditional stability criteria (3) into (4), we get the following condition:

$$((1 - \cos\theta)|FD| - 2 \cdot \text{Re}(J)\text{Re}(E)) \cdot r_0 \leq 2\text{Re}(z_m)\text{Re}(J)$$

If $(1 - \cos\theta)|FD| - 2\text{Re}(J)\text{Re}(E) \geq 0$

$$r_0 \leq V1 = \frac{2\text{Re}(z_m)\text{Re}(J)}{[(1 - \cos\theta)|FD| - 2\text{Re}(J)\text{Re}(E)]} \quad (5)$$

The product of position and force scaling, $r_0$ will have the upper bound as shown in (5), where

$$r_0 = s_p s_f,$$

$$D = \frac{G_c G_r}{1 + G_c G_r},$$

$$\theta = \angle(FD)$$

The other condition (1) can impose a constraint on the product of scalings $r_0$, since the $p_{11}$ in (4) should have a real part that is not negative. This leads to the following:

From (1), (4) $\quad \text{Re}(\frac{1}{G_m} + r_0 E) > = 0$

If $\text{Re}(E) > 0$, then $r_0 \geq -\frac{\text{Re}(1/G_m)}{\text{Re}(E)}$ (6a)

If $\text{Re}(E) < 0$, then $r_0 \leq -\frac{\text{Re}(1/G_m)}{\text{Re}(E)}$ (6b)

This means that if the real part of E is positive, the product of scaling has a lower bound. Therefore, in our control architecture the product of scaling $r_0$ is constrained by the conditions of (1) and (3).

The H matrix as shown above is not reciprocal. Hence, there exists some difference between the passivity criteria and unconditional stability(Adams and et. al., 1999).

In the simulation, we used a first order model for both the M and S, with the slave force filter $g_f$ =0 for simplicity. A PI type global controller for velocity (see Fig. 2 caption) was used. We fixed all gains(ex, $s_f$=1) except $s_p$ during the simulation. The simulation result of the upper bound of scaling is shown in Fig. 2. Figure 2(b) shows three kinds of upper bounds for stable $r_0$ based on (a) LL's first condition, (b) LL's third condition, (c) the passivity condition. The upper bound of scaling based on LL's condition is about 8 (for w >=1.5 rad/sec), while the passivity condition shows an upper bound of 5.9. Here we should note that the scaling bound depends on the frequency. In this case, the zero crossing point is shown at the frequency of 1.5 [rad/sec], below which $r_0$ has a lower bound of a negative value. This can be explained by (6a), (6b), and Fig. 2(c), (d). Since we assumed $r_0$ to be positive for normal forward $s_p$ and feedback $s_f$, any positive $r_0$ satisfies (1).

In the following section we want to check the sampling rates and inherent time delay effects on
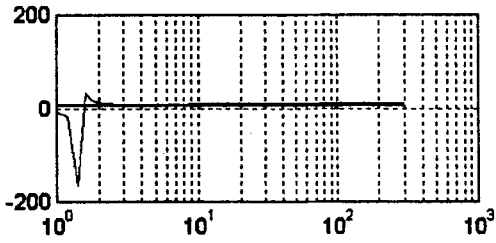
(a)  Upper bound of scaling(ro=sp*sf)
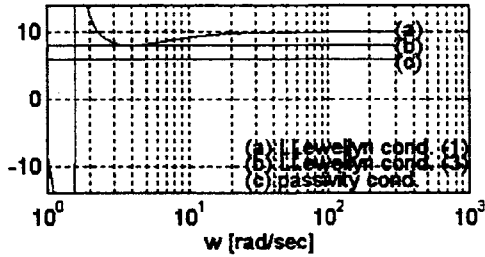


(b)  Magnified view of a) in y axis
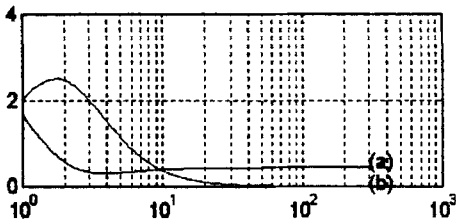


(c)  Real(h11) : (a) & real(h22) : (b)
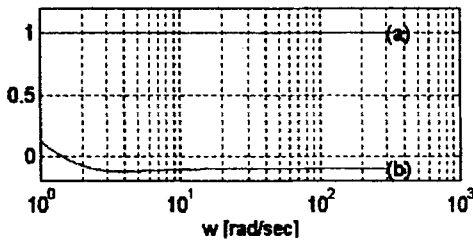


(d)  Real(11Gm) : (a) & real(E) : (b) for Llewellyn cond. 1

**Fig. 2**  Simulation result of upper bound of scaling:
(a) Several scaling bounds, (b) Magnified
view of (a), (c) Real part of h11(s) and
h22(s), (d) Real part of 1/Gm(s) and E with
sf=1, gp=1, gf=0, Master plant(m=1, b=
1), Slave plant(m=0.1, b=0.5), Gc=bc+kc/
s,(bc=−0.1, kc=0.3)

the stability with position and force scaling by
simulation. This analysis is based on the pole
location criteria and the plant models of M, S that
is from our former experimental set up (Fig. A1).

Otherwise, we can expect many difficulties in
setting the appropriate gains of controller and
plants.

# 3. Scaling, Sampling Rates and Stability Based on Characteristic Equation

We used the following definition(Adams, 1999)
to derive the stability criteria of the 2 port model
of teleoperation.

**Definition** : A continuous (discrete) linear two-
port network with given terminal immitances is
stable if and only if the corresponding characteris-
tic equation has no roots in the right half s-plane
(outside the unit circle for the z-plane) and only
simple roots on the imaginary axis (unit circle).

### 3.1  Transfer function of digital control

For simplicity, a multiple of sampling time and
same time delays in the master and slave are
assumed. The H.O.'s force and environment exter-
nal force are the inputs to the system, while
position or velocity of the master and slave are
the outputs. The Forward flow (position/veloc-
ity) and backward effort (force) method is used
(Hannaford, 1989). The control law used is a
classical PD control (to position) for MS with
coordinate torques.

$$S_p x_m - x_s = S_p v_m - v_s = 0 \qquad (7)$$

$$\tau_c = k_{c1}(x_m - x_s) + b_{c1}(v_m - v_s) \qquad (8)$$

We derive the transfer function from human
operator force to slave position and master posi-
tion in the Z domain. From Fig. 3,

$$X_r^* = G_{rp}^* U_r^* = G_{rp}^*(b_r D^* X_r^* + F_c^*) \qquad (9)$$

where $X_r^*$ is the starred transform (Phillips and
Nagle, 1984) and is defined as

$$X_r^* = X_r^*(s) = \sum_{n=0}^{\infty} X_r(nT)e^{-nTs}$$

The control input coordinating torque for the
MS is

$$F_c^* = (k_c S_p + b_c S_p D^*)X_m^* - (k_c + b_c D^*)X_r^* \qquad (10)$$

The sampled master position is

$$X_m^* = G_{mp}^* U_m^*$$
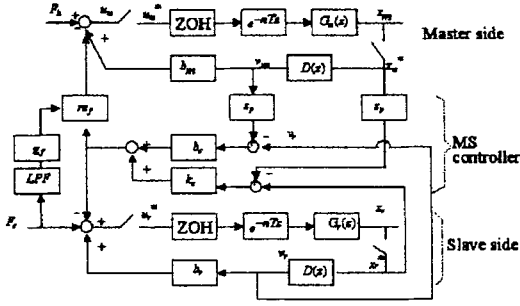
**Fig. 3** Block diagram of 1DOF system for sampling rate simulation, scaling and stability with ZOH

$$= G_{mp}^*(F_h^* + b_m D^* X_m^* - rs_f F_c^*) \qquad (11)$$

From (11)

$$X_m^* = \frac{G_{mp}^*(F_h^* - rs_f F_c^*)}{1 - G_{mp}^* b_m D^*} \qquad (12)$$

The coordinating torque is

$$F_c^* = h_1 X_m^* - h_2 X_r^* = h_2(s_p X_m^* - X_r^*) \qquad (13)$$

where

$$h_1 = k_c s_p + b_c s_p D^* = s_p h_2, \quad h_2 = k_c + b_c D^*$$

Substituting (12) into (13)

$$F_c^* = h_1 \left( \frac{G_{mp}^*}{1 - G_{mp}^* b_m D^*} F_h^* - \frac{rs_f G_{mp}^*}{1 - G_{mp}^* b_m D^*} F_c^* \right) - h_2 X_r^*$$

$$= h_1(h_3 F_h^* - h_4 F_c^*) - h_2 X_r^* \qquad (14)$$

where $h_3 = \dfrac{G_{mp}^*}{1 - G_{mp}^* b_m D^*}$, $h_4 = \dfrac{rs G_{mp}^*}{1 - G_{mp}^* b_m D^*}$

From (14)

$$F_c^* = g_1 F_h^* - g_2 X_r^* \qquad (15)$$

where $g_1 = \dfrac{h_1 h_3}{1 + h_1 h_4}$, $g_2 = \dfrac{h_2}{1 + h_1 h_4}$

Substituting (15) into (9)

$$X_r^* = G_{rp}^* b_r D^* X_r^* + G_{rp}^*(g_1 F_h^* - g_2 X_r^*) \qquad (16)$$

From (16)

$$T_{hr}^*(s) = \frac{X_r^*(s)}{F_h^*(s)} = \frac{g_1 G^*_{rp}}{1 + g_2 G^*_{rp} - b_r D^* G^*_{rp}}$$

$$= \frac{(h_1 h_3) G^*_{rp}}{(1 + h_1 h_4) + h_2 G^*_{rp} - (1 + h_1 h_4) b_r D^* G^*_{rp}} \qquad (17)$$

From (17), we can get the following expression:

$$T_{hr}^*(s) = \frac{(s_p G_c) G^*_{mp} G^*_{rp}}{(L_m + s_p s_f r G_c G_{mp}^*) \cdot L_r - G_c G_{rp}^* L_m} \qquad (18)$$

where $G_c$: coordinated control for MS

$$G_c = k_c + b_c D^*$$

$L_m$: loop transfer function around master

$$L_m = 1 - b_m D^* G^*_{mp}$$

$L_r$: loop transfer function around slave

$$L_r = 1 - b_r D^* G^*_{rp}$$

We can find $T_{hr}(z) = \dfrac{N_{hr}(z)}{D_{hr}(z)}$ from (17) (a detailed derivation is in the Appendix). From the denominator of (18), the product, $r_0(=sp^*sf)$ is shown. We can plot the root locus of the system about $r_0$.

### 3.2 Plant models for simulation

In this section the master and slave plant models in the Z-domain are introduced.

#### 3.2.1 Master plant model

The master to be modeled is a one DOF handle with a motion range of 180 degrees, and a 150 mm long arm driven by a brushed DC servo motor having 5.65 NM maximum torque(the right side of Appendix Fig. A1). The digital control model for the master is derived as follows:

$$G_{mp}(s) = zoh \cdot TimeDelay \cdot Plant$$
$$= \frac{1 - e^{-Ts}}{s} \cdot e^{-sT_d} \frac{K_1 K_2}{s(J_m s + B_m)} \qquad (19)$$

where $J_m = 3.04$ [Nms²/rad],
$\qquad B_m = 0.156$ [Nms/rad]

The complete digital control model was built by a Z-transform of (19) (see Appendix).

#### 3.2.2 Slave plant model

The slave plant to be modeled is a flat-coil magnetic head position actuator from a 1.8 incl hard disk drive of $1.18 \times 10^{-3}$ Nm maximum torque, which is 1/4790 of the master actuator. The slave has a 40 degree motion range with a 30 mm long head arm. We used a second order plant for the slave to reflect the spring effect from the printed circuit cable attached to the head arm.

$$G_{sp}(s) = \left[ \frac{1 - e^{-Ts}}{s} \right] e^{-sTd} \left[ \frac{k_3 k_4}{J_r s^2 + B_r s + K_r} \right] \qquad (20)$$

where $J_r = 2.39 \times 10^{-7}$ [Nms²/rad],
$\qquad B_r = 1.35 \times 10^{-5}$ [Nms/rad],
$\qquad K_r = 4.15 \times 10^{-4}$ [Nm/rad]

### 3.3 Characteristic equation and its order

The characteristic equation, the denominator of (12), depends on the MS plants, global and local control, scaling gains of $s_p$, $s_f$, sampling rates and the assumed time delay. In this work the communication time delay between the master and slave is not considered because of short distance. However, there is some time delay due to the sampled control system, resulting in some time duration between measuring the data and output of the actuator signal. This is believed to be one or two sampling time durations in a single system with some randomness. As the time delay increases by 1 Ts, the order of the global system increases by 2.

## 4. Simulation Results

### 4.1 Root Locus of position scaling and force scaling

To see the effects of position and force scaling gains, $s_p$ and $s_f$ we arrange the characteristic equation from (18) as

$$1 + s_p \frac{N_a(z)}{D_a(z)} = 0$$

$$1 + s_f \frac{N_b(z)}{D_b(z)} = 0$$

Figure 4 shows the root locus of the sp gain from 0.1 to 10 when the sampling rate and force scaling are fixed at 1KHz and 4550, respectively. Here $s_p$ of less than 1 means contractive positioning from the master to slave. The characteristic

equation Da(z) has 6 poles with no time delay condition. It is shown that one pole pair goes unstable as sp increases. We observed this pole pair moving while varying the force scaling sf and sampling rate since the other poles stay inside the unit circle of the Z-domain. Figure 5 shows the root locus of sf when the sampling rate and position scaling are fixed at 1KHz, and $s_p = 1$.

The pole moving pattern is similar to $s_p$, but there is a difference in sensitivity.

### 4.2 Stable scaling zone

Table 1 shows the simulation cases for varying the sampling rate and assumed time delay. Time delays in each M and S are assumed from 0 to 3 Ts. Five cases of sampling rates from 1 KHz to 60 Hz are simulated.

The simulation results for no time delay are shown in Fig. 6(a)-(d) where the horizontal plane is the operation region of the position scaling $s_p$ and force scaling $s_f$ and the Z-axis is the sampling time, Ts(1/sampling rate). Each

**Table 1** Case classification for simulation

| Fs        Td | 0 Ts  | 1 Ts  | 2 Ts  | 3 Ts  |
|--------------|-------|-------|-------|-------|
| Sys. order   | 6     | 8     | 10    | 12    |
| Case (a)     | 1 KHz | 1 KHz | 1 KHz | 1 KHz |
| Case (b)     | 500 Hz| 500   | 500   | 500   |
| Case (c)     | 250 Hz| 250   | 250   | 250   |
| Case (d)     | 125 Hz| 125   | 125   | 125   |
| Case (e)     | 60 Hz | 60    | 60    | 60    |
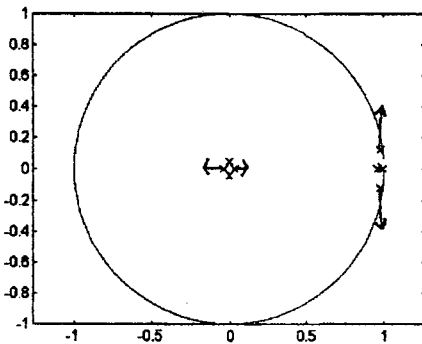


**Fig. 4** Z domain Root locus of 8$^{th}$ order system with 1 Ts delay and varied position scaling (0.1~10)
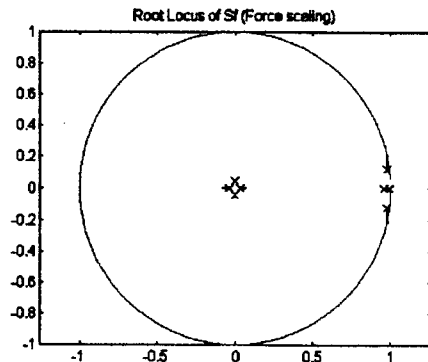


**Fig. 5** Root locus of force scaling, $s_f$ with 1Ts time delay, 1KHz, and $s_p = 1$ as $s_f$ varies from 455 to 4550 showing 8 poles moving
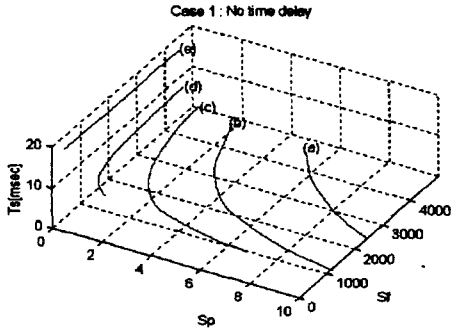
**Fig. 6(a)** Stable scaling zone of position and force with no time delay showing wider feasible range
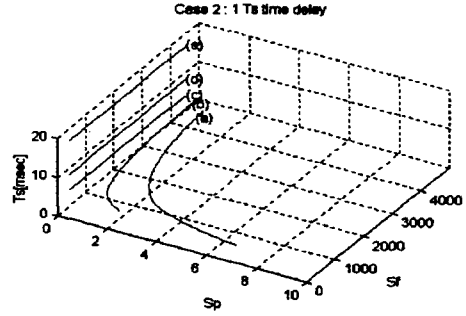


**Fig. 6(b)** Stable scaling zone of position and force with 1 sampling time delay showing shrinkage of feasible domain
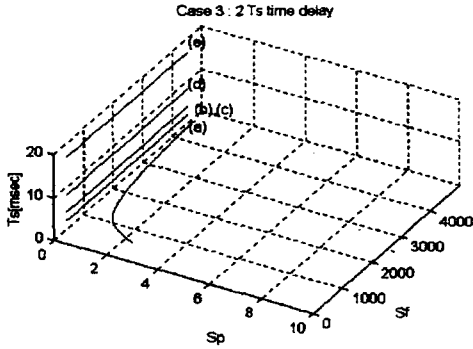


**Fig. 6(c)** Stable scaling zone of position and force with 2 sampling time delay
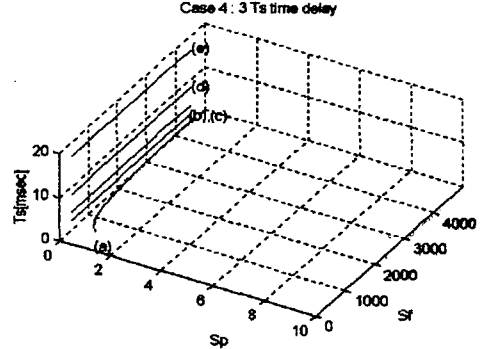


**Fig. 6(d)** Stable scaling zone of position and force with 3 sampling time delay

curve in Fig. 6(a) is the boundary of the stability region. The upper right corner of the curve is the unstable region, while the lower left corner is stable in the plane of constant Ts when $s_p$ is on the x-axis and $s_f$ is on the y-axis.

## 5. Conclusion

In Sec. 2, we derived the upper bound of $r_0$ (product of position and force scaling) using Llewellyn's unconditional stability which shows a 25% larger value than the passivity condition in a simple first order model of the master and slave. This confirms the less conservative feature of Llewellyn's condition in a non-reciprocal system. We confirm that the value of the scaling product $r_0$ can be an index of the system stability supported by (Hwang, et. al., 1994 and Daniel, et. al., 1998). Daniel and McAree (1998) added two more indices of the slave natural frequency and

mass ratio of the master and slave in the s-domain to the stability criterion. In the scaled teleoperation, the feasible region of scalings of position and force should be known for several reasons such as safety, full use of the system, etc.

From the viewpoint of implementation, a teleoperation system is cascaded, multi-dynamics based and computer controlled. Hence, the sampling rates and the inherent time delay from the sample and hold of a digital control system regardless of communication channel time delay deserves attention. We derived a transfer function between the human operator and the slave position in the Z-domain. We can summarize the simulation results from Sec. 3 and 4 as

• It is shown that the rather large change occurs in the stable region of the scaling factors sp and sf depending on the assumed time delay. This can affect the operation and safety of teleoperation. The randomness and exact time delay in a
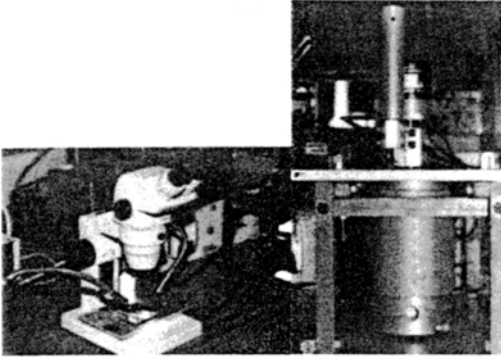
**Fig. A1**  Scaled telemanipulation system used for the simulation based on characteristic equation of digital control

computer control system should be studied further.

- Increase of one sampling time delay in both the master and slave leads to second-order terms in the system dynamics.
- The stability based on the characteristic equation of Thr(z) is a SISO rather than MIMO system. Hence, $r_0$ from Thr(z) can be less conservative than $r_0$ from unconditional stability.

## Appendix

The master and slave plant models including sample and hold in the Z-domain are derived as follows:

$$G_{mp}(s) = zoh \cdot TimeDelay \cdot Plant$$

$$= \frac{1-e^{-Ts}}{s} \cdot e^{-sT_0} \frac{k_1 k_2}{s(J_m s + B_m)}$$

$$= \frac{1-e^{-Ts}}{s} \cdot e^{-sT_0} \frac{K_m}{s(s+a)}$$

where $K_m = \dfrac{k_1 k_2}{J_m}$, $a = \dfrac{B_m}{J_m}$

$$= (1-e^{-Ts}) \cdot (e^{-sT_0}) \cdot \left(\frac{K_m}{s^2(s+a)}\right)$$

$$= G_1^* \cdot G_2^* \cdot G_3$$

$$G_{mp}(z) = G_1(z) \cdot G_2(z) \cdot G_3(z)$$

where $T_0$ is $n \cdot T_s$

$$G_1(z) = \frac{z-1}{z}$$

$$G_2(z) = z^{-n}$$

$$G_3(z) = \left(\frac{k_m}{a}\right)\left[\frac{Tz}{(z-1)^2} - \frac{(1-e^{-aT})z}{a(z-1)(z-e^{-aT})}\right]$$

$$G_{sp}(s) = \left(\frac{1-e^{-Ts}}{s}\right)e^{-sTd}\left(\frac{k_3 k_4}{Js^2 + Bs + K}\right)$$

$$= G_4 G_5 G_6$$

$$= G_4^* G_5^* G_6$$

where $G_4 = \dfrac{1-e^{-Ts}}{s}$, $G_5 = e^{-sTd}$,

$$G_6 = \left(\frac{k_3 k_4}{Js^2 + Bs + K}\right)$$

$$G_{sp}(z) = G_4(z) \cdot G_5(z) \cdot G_6(z)$$

$$= (1-z^{-1})z^{-n}z\left(\frac{k_3 k_4}{s(s^2 + B_2 s + K_2)}\right)$$

where $k_{r2} = (k_3 k_4)/J$, $B_2 = B/J$, $K_2 = K/J$

Now, deriving $G_{6a}(z) = z\left(\dfrac{k_{r2}}{s(s^2 + B_2 s + K_2)}\right)$

## References

Adams, R.J., Hannaford, B., 1999, "Stable Haptic Interaction with Virtual Environments," *IEEE Transactions on Robotics and Automation*, Vol. 15, No. 3, pp. 465~474.

Anderson, R. J. and Spong, M., 1998, "Bilateral Control of Teleoperators with Time Delay," *Proc. IEEE Intl. Conf. Systems, Man & Cybernetics*, Vol. 1, pp. 131~138, Beijing, China.

Choi, B.H., Jung, W.J. and Choi, H.K, 1999, "Study for Control of Master-Slave Teleoperation System with Time Delay," *KSME*, Vol. 23 A, pp. 57~65.

Colgate, J.E., 1994, "Coupled Stability of Multip ort Systems-Theory and Experiments," *Trans. ASME, Journal of Dynamic Systems, Measurement, and Control*, Vol. 116, No. 3, pp. 419~28.

Colgate, J. Edward, 1991, "Power and Impedance Scaling in Bilateral Manipulation," *IEEE Intern. Conf. on Robotics and Automation*, Sacramento, California.

Daniel, R.W., and McAree, P.R., 1998, "Fun-

damental Limits of Performance for Force Reflecting Teleoperation," *International Journal of Robotics Research*, Vol. 17 , No. 8, pp. 811~830.

Fukuda, T. Tanie, K. and Mitusuoka, T., 1987, "A New Method of Master-slave Type of Teleoperation for a Micro-Manipulator System," *IEEE Micro Robots and Teleoperators Workshop*, Hyannis, Massachusetts.

Hannaford, B., 1989, "Design Framework for Teleoperators with Kinesthetic Feedback," *IEEE Transactions on Robotics and Automation*, Vol. 5, No 4.

Hwang, D.Y., and Hannaford, B., 1994, "Modeling and Stability Analysis of a Scaled Telemanipulation System," *IEEE International Workshop on Robot and Human Communication*, pp. 32~37.

Hwang, D.Y., and Hannaford, B., 1998, "Teleoperation Performance with Kinematically Redundant Slave Robot," *International Journal of Robotics Research*, Vol. 17 , No. 6, pp. 579~597.

Kim, Won S., 1992, "Developments of New Force Reflecting Control Schemes and an Application to a Teleoperation Training Simulator," *IEEE Intern. Conf. on Robotics and Automation*, pp. 1412~1419, Nice, France.

Kobayashi, H., and Nakamura, H., 1992, "A Scaled Teleoperation," *IEEE International Workshop on Robot and Human Communication*, pp. 269~274.

Lawn, C.A. and Hannaford, B., 1993, "Performance Testing of Passive Communication and Control in Teleoperation with Time Delay," *IEEE Intern. Conf. on Robotics and Automation*, Vol. 3, pp. 776~781. Atlanta, GA.

Lawrence, Dale A., 1993, "Stability and Transparency in Bilateral Teleoperation," *IEEE Transactions on Robotics and Automation*, Vol. 9, No. 5.

Phillips, C.L. and Nagle, H.T., Jr., 1984, *Digital Control System Analysis and Design*, Prentice-Hall. Englewood Cliffs, N.J.

Raju, G.J., Verghese, G.C. and Sheridan, B., 1989, "Design Issue in 2-Port Network Models of Bilateral Remote Teleoperation," *Proc. IEEE Intl. Conf. Robotics and Automation*, pp. 1317~1321.

Strassberg, Y., 1992, "A Control Method for Bilateral Teleoperating Systems," Ph.D. Thesis, Dept. of Mech., Univ. of Toronto.

Yokokohji, Y., Hosotani, N. and Yoshikawa, T., 1994, "Analysis of Maneuverability and Stability of Micro-Teleoperation Systems," *IEEE Conf. R&A.*